Long-Term Foundation Response to Repetitive Loading

Cesar Pasten, A.M.ASCE[1]; Hosung Shin[2]; and J. Carlos Santamarina[3]

Abstract: Repetitive loading can induce volumetric and shear strain accumulation in soils and affect the long-term performance of engineered and natural geosystems. A hybrid numerical scheme based on the FEM is implemented to analyze problems where a very large number of cycles is involved. The numerical approach combines a classical mechanical constitutive model to simulate the static load and the first load cycle and empirical accumulation functions to track the accumulation of deformations during repetitive loading. The hybrid model captures fundamental characteristics of soil behavior under repetitive loading, such as threshold strains, terminal density, and ratcheting response; it also predicts volumetric and shear strains as a function of the static stress obliquity, the number of load cycles, and the plastic strain during the first load cycle. The proposed numerical scheme is used to analyze shallow foundations subjected to repetitive loads. Results show the evolution of vertical settlement, horizontal displacement, footing rotation, and stress redistribution within the soil mass as the number of load cycles increases. Displacements and rotation are more pronounced as the static factor of safety decreases and the cyclic load amplitude increases. **DOI: 10.1061/(ASCE)GT.1943-5606.0001052.**

Author keywords: Repetitive load; Threshold strains; Terminal density; Finite-element method (FEM); Footing.

Introduction

Repetitive boundary loads can induce volumetric and shear strain accumulation in soils. Cumulative deformations reflect the static and cyclic stress fields, drainage and frequency effects, and the number of repetitions.

The long-term behavior of granular materials subjected to repetitive boundary conditions can be captured with classical constitutive models. Examples of mechanical models that describe the complete stress-strain response of a material include bounding surface plasticity (Dafalias and Herrmann 1986), kinematic hardening (Mróz 1967), generalized plasticity (Zhang et al. 2001), and combined formulations (Gajo and Muir Wood 1999). Constitutive models with irreducible plastic potentials during unloading are not suitable to simulate strain accumulation because of their inability to predict plastic strain upon reloading. In general, the use of classical constitutive models requires major computational resources when the number of load repetitions is high, and the accumulation of numerical errors may distort the predicted deformations (Niemunis et al. 2004).

Empirical strain accumulation functions have been proposed to fit experimental results as a function of the number of load cycles. Accumulation functions can be divided into three groups:

1. Equations that describe one component of the accumulated strain as a function of the first load cycle, the number of cycles, the static state of stress, and the initial density (Diyaljee and Raymond 1982; Gidel et al. 2001; Lentz and Baladi 1981; Sawicki and Swidzinski 1989; Sweere 1990; Tseng and Lytton 1989);
2. Equations that predict one component of the accumulated strain at a reference number of cycles N_{ref} as a function of the state of stress, the initial void ratio, and the static shear strength (Barksdale 1972; Brown 1974; Lekarp and Dawson 1998; Lentz and Baladi 1980); and
3. Equations that predict the complete evolution of strain accumulation (i.e., magnitude and direction) as a function of the number of cycles, the state of stress, and the initial density (Bouckovalas et al. 1984; François et al. 2010; Kaggwa et al. 1991; Marr and Christian 1981; Niemunis et al. 2005; Suiker and de Borst 2003).

While strain accumulation functions are stable, their standalone application is restricted to simple boundary conditions.

This study advances a stable deformation accumulation algorithm to analyze the long-term response of geotechnical structures subjected to repetitive loading. The methodology builds on previous developments by others (Suiker and de Borst 2003; Niemunis et al. 2005; François et al. 2010). (Note: a comparative analysis is presented later in the Discussion section.) The hybrid approach involves a classical mechanical constitutive model to analyze the static load and the first load cycle and to satisfy equilibrium and compatibility during repetitive loading. In addition, empirical strain accumulation functions are invoked to estimate strain accumulation during repetitive loading. This manuscript starts with a review of soil behavior under repetitive mechanical loading, followed by a description of the proposed numerical scheme and field examples.

Soil Behavior under Repetitive Loading

The analysis of the long-term response of geotechnical systems subjected to repetitive loading is fraught by the large number of variables involved and by constitutive parameters that are difficult to calibrate. We seek to develop a robust numerical scheme that properly reflects salient features of soil behavior under repetitive loading with a limited number of parameters.

[1]Assistant Professor, Dept. of Civil Engineering, Univ. of Chile, Santiago, 8370449, Chile (corresponding author). E-mail: cpasten@ing.uchile.cl

[2]Assistant Professor, School of Civil and Environmental Engineering, Univ. of Ulsan, Ulsan 680-749, Republic of Korea. E-mail: shingeo@ulsan.ac.kr

[3]Professor, School of Civil and Environmental Engineering, Georgia Inst. of Technology, Atlanta, GA 30332. E-mail: jcs@gatech.edu

Note. This manuscript was submitted on February 19, 2013; approved on October 7, 2013; published online on December 2, 2013. Discussion period open until May 2, 2014; separate discussions must be submitted for individual papers. This paper is part of the ***Journal of Geotechnical and Geoenvironmental Engineering***, © ASCE, ISSN 1090-0241/04013036(11)/$25.00.

Threshold Strains

Particle-level deformation mechanisms change with strain level. If the cyclic strain level is below the elastic threshold strain, the soil deforms at grain contacts without slippage (Dobry and Swiger 1979; Santamarina et al. 2001). In contrast, the soil undergoes particle rearrangement and fabric changes when the strain level exceeds the volumetric threshold strain. At this strain level, the soil experiences either plastic volumetric strain in drained conditions or changes in pore pressure and mean effective stress in undrained conditions (Vucetic and Dobry 1991).

Ratcheting, Shakedown, and Terminal Density

The long-term response of geomaterials subjected to repetitive loading can be characterized by either ratcheting or shakedown behavior. Ratcheting is the sustained long-term accumulation of shear strain during repetitive loading; typically, it develops under high stress obliquity (Alonso-Marroquin and Herrmann 2004). In contrast, when strain accumulation decreases toward an asymptotic value (i.e., the plastic strain increment per cycle becomes null), the soil reaches a stable deformation state known as shakedown (Garcia-Rojo and Herrmann 2005).

When the initial cyclic strains are larger than the elastic threshold strain, the soil fabric gradually evolves toward a statistically stable structure characterized by its terminal density, or terminal void ratio (Narsilio and Santamarina 2008). The terminal density is process-dependent and sets the upper bound for volumetric strain accumulation, even if the material experiences particle breakage during repetitive loading. Note that terminal density is reached in both ratcheting and shakedown behavior.

Cyclic Response in the Stress-Strain-Volume Space

The behavior of a granular material subjected to cyclic stress-controlled loading in triaxial conditions is schematically shown in Fig. 1(a). The soil response is characterized by the initial void ratio e_0, the initial static mean stress p_0, deviatoric stress q_0, and the cyclic stress amplitude Δq. (Note: we adopt octahedral definitions $p' = (\sigma'_{11} + \sigma'_{22} + \sigma'_{33})/3$ and $q = (3/2)^{1/2}[(\sigma'_{11} - p')^2 + (\sigma'_{22} - p')^2 + (\sigma'_{33} - p')^2 + 2(\sigma'_{12})^2 + 2(\sigma'_{13})^2 + 2(\sigma'_{23})^2]^{1/2}$.) The conceptual trends in Fig. 1(a) show high plastic deformation induced by the first load cycle, gradual strain accumulation in every cycle, a relatively constant elastic component of the deformation (q–ε_1 quadrant), and the soil asymptotically approaching terminal density (e–p' and e–ε_1 quadrants).

Fig. 1(b) depicts the evolution of the strain increment per cycle as a function of the number of load cycles for soil specimens subjected to three different initial stress obliquities $\eta_0 = q_0/p'_0$. The arrows represent the incremental plastic strain vector per load cycle. The horizontal and vertical components reflect the volumetric $\varepsilon_v|_i$ and the shear $\varepsilon_q|_i$ strain changes per cycle. The plastic strain in the first load cycle exhibits volumetric $\varepsilon_v|_{i=1}$ and shear components $\varepsilon_q|_{i=1}$ and is normal to the monotonic plastic potential, such as the modified Cam clay yield surface shown in the figure (Chang and Whitman 1988; Lackenby 2006; Suiker et al. 2005; Wichtmann et al. 2006, 2010b). The soil element subjected to an initial state of stress close to the critical state line $\eta = M$ (shown as state S1) accumulates mainly shear strain, and its increment per cycle gradually becomes constant as the number of cycles increases. In contrast, the soil element subjected to an initial nearly isotropic state of stress (shown as state S3) experiences mainly volumetric strain accumulation, and the strain increment per cycle goes to zero as the material approaches its terminal void ratio e_∞.

Numerical Modeling of Boundary Value Problems

A numerical scheme is developed herein to analyze geotechnical systems that experience long-term repetitive loading. The algorithm

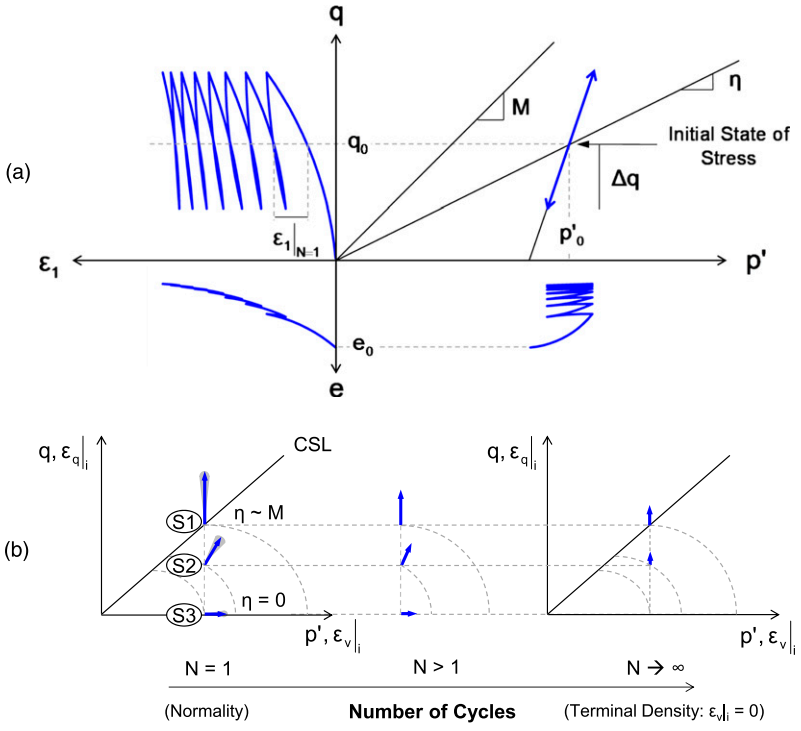

Fig. 1. Behavior of a granular material subjected to drained cyclic triaxial loading: (a) evolution of effective mean stress p', deviatoric stress q, axial strain ε_1, and void ratio e; (b) evolution of the strain increment per cycle with the number of load cycles; S1, S2, and S3 are initial stress states

J. Geotech. Geoenviron. Eng. 2014.140.

is framed within a finite-element formulation and considers the soil behavior trends described previously. Vectors are expressed in bold lowercase letters and matrices in bold uppercase letters.

Algorithm for Long-Term Repetitive Loading

The proposed algorithm involves four modules. These modules and the selected constitutive functions are described herein.

Module #1: Initial Static Condition

The stress field induced by self-weight and the initial static component of the applied load P_A are computed using the standard FEM and a selected mechanical constitutive model. At every integration point, the computed static stress is $\boldsymbol{\sigma}_{\mathrm{A}}$ and the corresponding strain is $\boldsymbol{\varepsilon}_{\mathrm{A}}$.

Module #2: First Load Cycle

The first load cycle is computed with the same constitutive model used in the previous module. The following stress $\boldsymbol{\sigma}' = (\sigma'_{xx}, \sigma'_{yy}, \sigma'_{zz}, \tau_{xy}, \tau_{xz}, \tau_{yz})^{\mathrm{T}}$ and strain $\boldsymbol{\varepsilon} = (\varepsilon_{xx}, \varepsilon_{yy}, \varepsilon_{zz}, \varepsilon_{xy}, \varepsilon_{xz}, \varepsilon_{yz})^{\mathrm{T}}$ vectors are obtained at every integration point (T denotes the transpose):

- $\boldsymbol{\sigma}'_B$ and $\boldsymbol{\varepsilon}_B$ at the maximum cycle load $P_{\max} = P_A + \Delta P$;
- $\boldsymbol{\sigma}'_C$ and $\boldsymbol{\varepsilon}_C$ after unloading to the minimum load $P_{\min} = P_A - \Delta P$; and
- $\boldsymbol{\sigma}'_D$ and $\boldsymbol{\varepsilon}_D$ after reloading to the initial static load P_A.

Note that the modified Cam clay model can be used only if the medium is normally consolidated or slightly overconsolidated after the initial static load so that the model can compute nonzero plastic strains for the first load cycle.

Subsequent load cycles will cause cyclic strain accumulation as long as the induced strain $(\boldsymbol{\varepsilon}_B - \boldsymbol{\varepsilon}_A)$ exceeds the elastic threshold strain $\boldsymbol{\varepsilon}_{\mathrm{e1}}$, which is a function of soil type and the confining stress. The plastic strain at the end of the first cycle is

$$\varepsilon^{D-A} = \varepsilon_D - \varepsilon_A \tag{1}$$

Hence, the volumetric and shear strains at the end of the first cycle are

$$\varepsilon_v|_{N=1} = \varepsilon_1 + \varepsilon_2 + \varepsilon_3\big|^{D-A} \tag{2}$$

and

$$\varepsilon_q\big|_{N=1} = \sqrt{2/3}\left[\left(\varepsilon_1 - \frac{\varepsilon_v|_{N=1}}{3}\right)^2 + \left(\varepsilon_2 - \frac{\varepsilon_v|_{N=1}}{3}\right)^2 + \left(\varepsilon_3 - \frac{\varepsilon_v|_{N=1}}{3}\right)^2 + 2(\varepsilon_4)^2 + 2(\varepsilon_5)^2 + 2(\varepsilon_6)^2\right]^{1/2}\Bigg|^{D-A} \tag{3}$$

The strains at the end of the first cycle inherently reflect the combined effects of the initial effective stress and the initial void ratio, the cyclic stress amplitude and direction, and the sediment prior stress history. If the modified Cam clay model is used, normality applies at the end of loading during the first cycle, in particular, $\varepsilon_v|_{N=1}(\eta = M) = 0$ and $\varepsilon_q\big|_{N=1}(\eta = 0) = 0$.

Module #3: Cyclic Strain Accumulation

The volumetric and shear strains that accumulate during repetitive cyclic loading are calculated using empirical accumulation functions. We sought simple, mechanics-informed functions to capture the main features of strain accumulation. Empirical equations for strain increments in the ith cycle and for cumulative strains after the Nth cycle are described next.

Strain Increments for the ith Cycle. The plastic volumetric strain per cycle vanishes as the sediment reaches terminal density, whereas the one-cycle plastic shear strain evolves toward a constant value. Then, volumetric and shear strain increments in the ith cycle are estimated as

$$\varepsilon_v|_i = \varepsilon_v|_{N=1}\left(\frac{a}{i}\right) \tag{4}$$

and

$$\varepsilon_q\big|_i = \varepsilon_q\big|_{N=1}\left(\frac{b}{i} + c\right) \tag{5}$$

where a, b, and c = constitutive parameters. The asymptotic values for $i \to \infty$ are $\varepsilon_v\big|_i = 0$ when the sediment reaches terminal density and $(\varepsilon_q\big|_{N=1} \cdot c)$ for the plastic shear strain increment; the parameter $c > 0$ corresponds to an element that experiences ratcheting.

Cumulative Strains after the Nth Cycle. The accumulated volumetric and shear strains after the Nth cycle are obtained by integrating Eqs. (4) and (5) from $i = 1$ to N

$$\varepsilon_v^{\mathrm{acc}}\big|_N = \varepsilon_v|_{N=1}[1 + a \cdot \ln(N)] \le \varepsilon_v^{\infty} \tag{6}$$

$$\varepsilon_q^{\mathrm{acc}}\Big|_N = \varepsilon_q\big|_{N=1}[1 + b \cdot \ln(N) + c \cdot (N-1)] \tag{7}$$

where ε_v^{∞} = cumulative volumetric strain the soil experiences when it changes from the initial void ratio e_A to the terminal void ratio e_∞

$$\varepsilon_v^{\infty} = \frac{e_A - e_\infty}{1 + e_A} \tag{8}$$

Eqs. (6) and (8) combine to predict the number of cycles needed to reach terminal void ratio N^*

$$N^* = \exp\left[\frac{1}{a}\left(\frac{e_A - e_\infty}{1 + e_A}\frac{1}{\varepsilon_v|_{N=1}} - 1\right)\right] \tag{9}$$

Note that the number of cycles to reach terminal void ratio N^* increases as the volumetric strain in the first cycle $\varepsilon_v\big|_{N=1}$ decreases (as shown in Narsilio and Santamarina 2008).

These accumulation functions predict trends that are asymptotically compatible with the sediment behavior reviewed earlier (sketched in Fig. 1). The volumetric strain accumulation for a soil element with an average stress obliquity close to critical state is null because $\varepsilon_v\big|_{N=1}(\eta_{av} = M) = 0$. In contrast, a soil element with an average stress obliquity close to the isotropic state does not accumulate shear strain given that $\varepsilon_q\big|_{N=1}(\eta_{av} = 0) = 0$. For any other stress obliquity and at a very high number of cycles, the shear strain continues accumulating linearly $\varepsilon_q^{\mathrm{acc}}\big|_N = \varepsilon_q\big|_{N=1} \cdot c \cdot (N-1)$, while volumetric strain accumulation gradually ceases.

Constitutive Parameters. The accumulation equations multiply the plastic strains in the first cycle, $\varepsilon_v\big|_{N=1}$ and $\varepsilon_q\big|_{N=1}$, so strain accumulation is inherently affected by the initial void ratio e_A, the initial static mean p_A and deviatoric q_A stresses, and the cyclic mean $\Delta p'$ and deviatoric Δq stress amplitudes. Experimental data show that constitutive parameters a, b, and c are mainly affected by the average stress obliquity $\eta_{av} = q_{av}/p'_{av}$, whereas other parameters have a secondary effect (see data in Wichtmann 2005). The initial average deviatoric stress q_{av} and mean stress p'_{av} are calculated using the stress field at the end of the first load cycle.

J. Geotech. Geoenviron. Eng. 2014.140.

Module #4: Compatibility and Equilibrium

Cumulative strains predicted for each element must satisfy compatibility, and the system must be in equilibrium throughout the domain, regardless of whether the soil elements experience cyclic strain accumulation (refer to Module #2).

Strain accumulation functions are not updated; thus, constitutive parameters (a, b, and c) and the strains in the first cycle, $\varepsilon_v|_{N=1}$ and $\varepsilon_q|_{N=1}$, remain constant. The additional volumetric and shear strains that accumulate from the cycle N to the cycle $(N + \Delta N)$ are

$$\Delta\varepsilon_v^{\text{acc}} = \varepsilon_v^{\text{acc}}|_{N+\Delta N} - \varepsilon_v^{\text{acc}}|_N \tag{10}$$

and

$$\Delta\varepsilon_q^{\text{acc}} = \varepsilon_q^{\text{acc}}|_{N+\Delta N} - \varepsilon_q^{\text{acc}}|_N \tag{11}$$

Both strains combine into the accumulated strain vector from plasticity

$$\Delta\varepsilon^{\text{acc}} = \frac{1}{3}\Delta\varepsilon_v^{\text{acc}}\mathbf{1} + \frac{3}{2}\frac{\Delta\varepsilon_q^{\text{acc}}}{q_N}\left(\boldsymbol{\sigma}'_N - p'_N \cdot \mathbf{1}\right) \tag{12}$$

where p'_N and q_N = mean and deviatoric stress components of the stress state $\boldsymbol{\sigma}'_N$ from the previous converged N-step and $\mathbf{1} = (1,1,1,0,0,0)^{\text{T}}$ = identity vector. (Note: although $\Delta\varepsilon_v^{\text{acc}}$ and $\Delta\varepsilon_q^{\text{acc}}$ depend on the static load and the first load cycle, the accumulation direction depends on the previously converged stress state $\boldsymbol{\sigma}'_N$.) The stress increment due to the accumulated strain $\Delta\varepsilon^{\text{acc}}$ is

$$\Delta\boldsymbol{\sigma} = \mathbf{D}^e \cdot (\Delta\varepsilon - \Delta\varepsilon^{\text{acc}} - \Delta\varepsilon^p) \tag{13}$$

where $\mathbf{D}^e[6\times 6]$ = elastic stiffness matrix, and the strains $\Delta\boldsymbol{\varepsilon}[6\times 1]$ and $\Delta\boldsymbol{\varepsilon}^p[6\times 1]$ = total and plastic strain increments induced to satisfy force equilibrium and strain compatibility through numerical iteration. The accumulated strain vector [Eq. (12)] induces internal stress $\Delta\boldsymbol{\sigma}$ [Eq. (13)] and unbalanced forces in the system. The iterative reduction in unbalanced forces during Newtonian iterations causes nodal displacements until the system reaches equilibrium.

If the modified Cam clay model is used to compute the static load and the first load cycle, the elastic stiffness matrix $\mathbf{D}^e$ is evaluated with the stress-dependent bulk modulus $B = (1 + e_N) \cdot p'_N/\kappa$ and a constant Poisson ratio ν. The void ratio e_N, the effective mean pressure p'_N, and the preconsolidation pressure pc'_N are obtained from the previous converged step N. The updated void ratio $e_{N+\Delta N}$ is calculated using the accumulated volumetric strain increment [Eq. (10)] and the updated preconsolidation pressure $pc'_{N+\Delta N}$ using the updated effective mean stress $p'_{N+\Delta N}$

$$e_{N+\Delta N} = e_N - (1 + e_N)\Delta\varepsilon_v^{\text{acc}} \tag{14}$$

$$pc'_{N+\Delta N} = \exp\left[\frac{N - \kappa\ln\left(p'_{N+\Delta N}\right) - e_{N+\Delta N}}{\lambda - \kappa}\right] \tag{15}$$

The void ratio at the end of the first cycle $e_{N=1}$ (Module #2) is the value after reloading e_D, and the preconsolidation pressure p'_{cN} is the cycle maximum load pc'_B.

Comments on Stability and Convergence

Fig. 2 summarizes the numerical algorithm. The stress field induced by the static load and the first load cycle (Modules #1 and #2) are spatially regular, as they inherently satisfy equilibrium and compatibility. Strains after N-cycles $\boldsymbol{\varepsilon}_N$ will be regular as long as the cyclic load amplitude ΔP is smaller than the static load P_A and the load cycle increments ΔN are advanced slowly during early cycles (low N values) to prevent numerical instabilities. The numerical scheme is advanced with increasingly larger load cycle increments ΔN until a target number of cycles N_f is reached.

1. Initial Static Condition: Self-Weight and Static Load (P_A)
   Calculated Strain: $\boldsymbol{\varepsilon}_A$
   Calculated Stress: $\boldsymbol{\sigma}_A$

2. First Load Cycle
   Calculated Strain: $\boldsymbol{\varepsilon}_B$, $\boldsymbol{\varepsilon}_C$, and $\boldsymbol{\varepsilon}_D$
   Calculated Stress: $\boldsymbol{\sigma}_B$, $\boldsymbol{\sigma}_C$, and $\boldsymbol{\sigma}_D$
   $\boldsymbol{\varepsilon}^{D\text{-}A} \rightarrow \varepsilon_v|_{N=1}$ and $\varepsilon_q|_{N=1}$ Eqs. (2) and (3)
   $\boldsymbol{\sigma}_D \rightarrow \eta_{av} = q_D/p'_D$
   $\boldsymbol{\sigma}_{N=1} = \boldsymbol{\sigma}_D$

3. Accumulated Strain Increment
   $\Delta\boldsymbol{\varepsilon}^{\text{acc}} = f(\Delta\varepsilon_v^{\text{acc}}, \Delta\varepsilon_q^{\text{acc}}, \boldsymbol{\sigma}_N)$ Eq.(12)
   where
   $\Delta\varepsilon_v^{\text{acc}} = \varepsilon_v^{\text{acc}}|_{N+\Delta N} - \varepsilon_v^{\text{acc}}|_N$
   $\Delta\varepsilon_q^{\text{acc}} = \varepsilon_q^{\text{acc}}|_{N+\Delta N} - \varepsilon_q^{\text{acc}}|_N$
   $\varepsilon_v^{\text{acc}}|_N = \varepsilon_v|_{N=1}[1 + a(\eta_{av})\ln(N)]$
   $\varepsilon_q^{\text{acc}}|_N = \varepsilon_q|_{N=1}[1 + b(\eta_{av})\ln(N) + c(\eta_{av})]$

4. Compatibility and Equilibrium
   Calculated Strain: $\boldsymbol{\varepsilon}_{N+\Delta N}$
   Calculated Stress: $\boldsymbol{\sigma}_{N+\Delta N}$

5. Increase Number of Cycles by ΔN if $(N+\Delta N) < N_f$
   Return to 3

Fig. 2. Flowchart of the numerical algorithm; the current number of cycles is N and the final number of load cycles is N_f

Numerical Examples

The hybrid algorithm described previously is implemented using the UMAT subroutine in *ABAQUS 6.10/Standard* with an explicit integration scheme so that the current step is calculated with values from the previous converged step. We select the modified Cam clay constitutive model to analyze the static load (Module #1) and the first load cycle (Module #2) and to satisfy equilibrium and compatibility during repetitive loading (Module #4).

Calibration

For this exploratory study, the model is calibrated using published triaxial test results for a quartzitic subangular sand (Wichtmann 2005). The sand critical state friction angle is $\varphi = 31.2°$ (i.e., $M = 1.25$), the minimum and maximum void ratios are $e_{\min} = 0.577$ and $e_{\max} = 0.874$, the mean grain diameter is $d_{50} = 0.55$ mm, and the coefficient of uniformity is $C_u = 1.8$. In the absence of experimental soil-specific data, the elastic threshold strain is estimated by assuming that interparticle displacement must exceed the atomic scale to break bonds $\|\boldsymbol{\varepsilon}_{e1}\| = 1\text{Å}/d_{50}$; therefore, both volumetric and shear elastic threshold strains for this sand are assumed to be $\varepsilon_{v,e1} = \varepsilon_{q,e1} = 10^{-7}$. Furthermore, in the absence of empirical data, we select the minimum void ratio $e_{\min}$ as the terminal void ratio e_∞ for the empirical accumulation functions in Module #3.

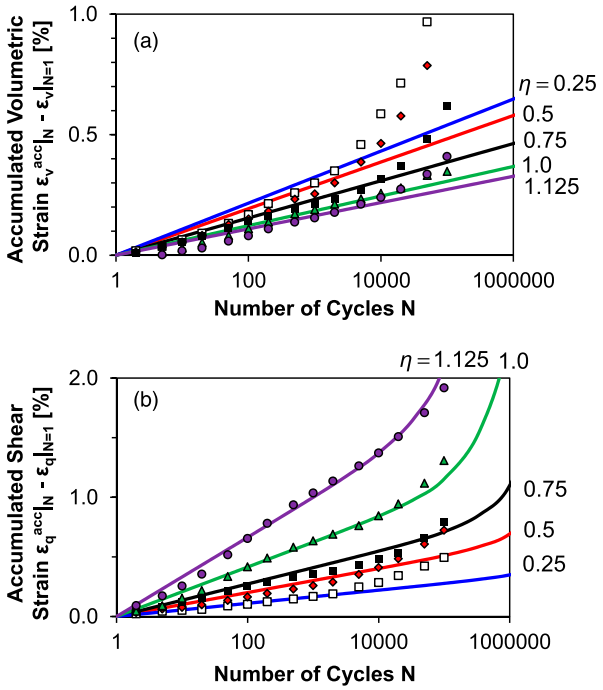

Fig. 3. Calibration of the accumulation functions using drained cyclic triaxial test results for stress obliquities $\eta = 0.25$ (open square), 0.5 (diamond), 0.75 (solid square), 1.0 (triangle), and 1.125 (circle): (a) accumulated volumetric strain; (b) accumulated shear strain; the average initial void ratio is $e_0 = 0.69$, the stress amplitude is $\Delta q = 60$ kPa, and the average mean stress is $p'_0 = 200$ kPa (data from Wichtmann 2005)

The effect of the average stress obliquity is considered by using the following constitutive parameters in Eqs. (6) and (7):

$$a(\eta_{av}) = a_1(M - \eta_{av})^2 + a_2 \quad (a_1 = 1.09 \text{ and } a_2 = 0.87) \quad (16)$$

$$b(\eta_{av}) = -b_1(\eta_{av}) + b_2 \quad (b_1 = 1.96 \text{ and } b_2 = 2.42) \quad (17)$$

$$c(\eta_{av}) = c_1(\eta_{av}) \quad (c_1 = 6 \cdot 10^{-6}) \quad (18)$$

Figs. 3(a and b) compare experimental data and calculated cumulative volumetric and shear strains. In linear-log scale, the measured volumetric strains show a pronounced increase after $N \sim 1{,}000$ cycles. This trend is unsustainable from a terminal-density point of view, as incremental volumetric strains must reach a zero asymptote. The apparent sustained growth of $\varepsilon_v^{acc}|_N - \varepsilon_v|_{N=1}$ in Fig. 3 is due to either an emergent deformation mechanism (e.g., fatigue breakage) or experimental difficulties (e.g., fines loss). Additional experimental data confirm that granular materials subjected to cyclic stress-controlled boundary conditions tend toward the terminal density corresponding to the imposed process for a large number of cycles (Kaggwa et al. 1991; Lackenby 2006; Rondón et al. 2009; Suiker et al. 2005; Youd 1972). Therefore, we opted to deviate from the volumetric strain data at large number of cycles when $N > 1{,}000$.

The number of cycles to reach terminal density N^* computed using Eq. (9) and the selected constitutive parameters (Table 1) shows that a soil element with initial void ratio $e_A = 0.70$ and average stress obliquity $\eta_{av} = 0.5$ reaches a terminal void ratio $e_\infty = e_{min} = 0.577$ after $N^* \sim 100{,}000$ load cycles if $\varepsilon_v|_{N=1} = 0.004$, and $N^* \sim 200$ cycles if $\varepsilon_v|_{N=1} = 0.008$.

Table 1. Soil Parameters in Numerical Examples

Parameter	Symbol	Value
Density	γ	18 kN/m^3
Coefficient of earth pressure at rest	K_0	0.586
Modified Cam clay		
Slope of unloading-reloading line in $e - \ln(p')$	κ	0.002
Poisson's ratio	ν	0.3
Slope of critical state line in $e - \ln(p')$	λ	0.004
Isotropic consolidation line at 1 kPa	N	0.71
Slope of critical state line in $p' - q$	M	1.25
Empirical accumulation functions		
Accumulated volumetric strain	a_1	1.09
	a_2	0.87
Accumulated shear strain	b_1	1.96
	b_2	2.42
	c_1	$6 \cdot 10^{-6}$

Note: The coefficient of earth pressure at rest is obtained from the compressibility parameters of the modified Cam clay model (details in Muir Wood 1990).

Physical Validation: Element Tests

Cyclic Triaxial Test

The cumulative axial strain and radial strain evolution with the number of load cycles N experienced by a soil element subjected to triaxial conditions are recovered from the volumetric and shear strain accumulation functions

$$\varepsilon_{radial}^{acc}|_N = \frac{1}{3}\left(\varepsilon_v^{acc}|_N - \varepsilon_v|_{N=1}\right) - \frac{1}{2}\left(\varepsilon_q^{acc}|_N - \varepsilon_q|_{N=1}\right) \quad (19)$$

and

$$\varepsilon_{axial}^{acc}|_N = \frac{1}{3}\left(\varepsilon_v^{acc}|_N - \varepsilon_v|_{N=1}\right) + \left(\varepsilon_q^{acc}|_N - \varepsilon_q|_{N=1}\right) \quad (20)$$

Fig. 4(a) shows the calculated trends for model parameters summarized in Table 1. An increase in the accumulated axial strain means vertical compaction, whereas a decrease in accumulated radial strain implies radial expansion. Both strains increase with stress obliquities, in agreement with Eqs. (16) to (18). (Note: The apparent acceleration with N is due to the logarithmic scale.)

Cyclic Loading under Zero-Lateral Strain

Experimental evidence shows that a soil element subjected to cyclic vertical load under zero-lateral strain conditions experiences volumetric strains and lateral stress changes (Sawicki and Swidzinski 1995). Fig. 4(b) shows a soil element consolidated to $\sigma_v = 100$ kPa and cyclically loaded with a stress amplitude $\Delta\sigma_v = 20$ kPa. The coefficient of earth pressure at rest $K_0 = \sigma_h/\sigma_v$ for virgin loading and the first unloading depends on the modified Cam clay model parameters in Table 1 and results in $K_0 = 0.62$. Assuming accumulation parameters summarized in Table 1, the value of K_0 decreases to a minimum value $K_0 = 0.58$ during the initial cycles and increases gradually toward the isotropic state for a large number of cycles. The void ratio decreases from the initial value $e_0 = 0.692$ to reach $e = 0.684$ after $N = 250{,}000$ cycles. For reference, the number of cycles to reach a terminal void ratio equal to $e_\infty = e_{min} = 0.577$ is $N^* \sim 10^{80}$ [from Eq. (9)]; however, it is unlikely that e_{min} is the terminal void ratio for zero-lateral-strain loading.

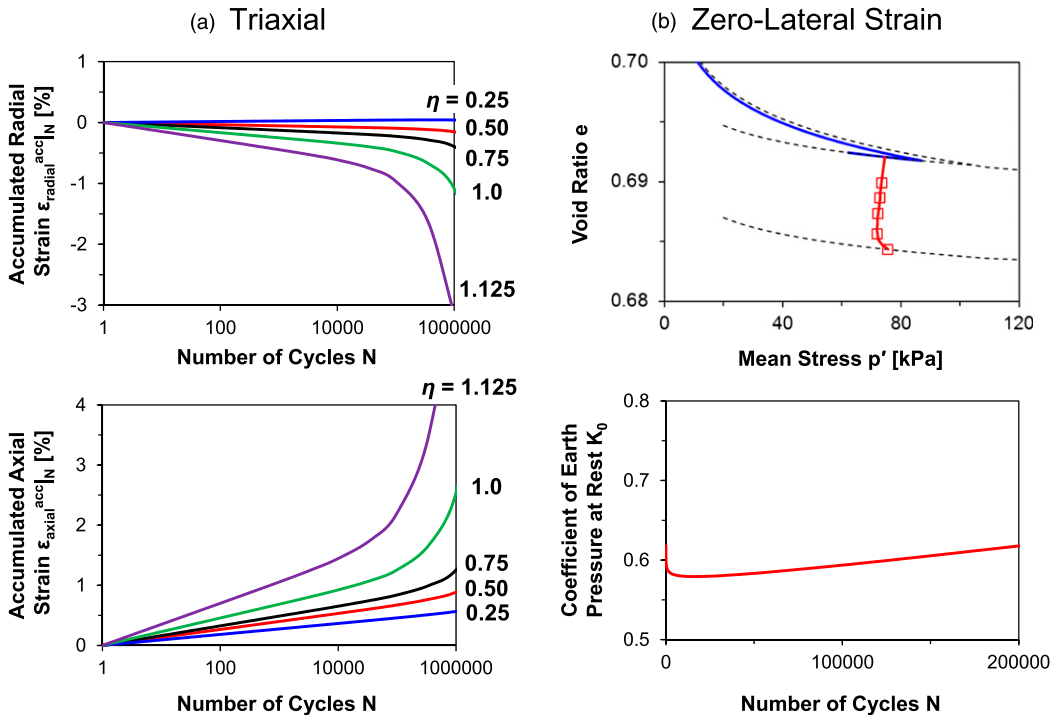

Fig. 4. Strain accumulation in element tests: (a) triaxial test: evolution of radial $\varepsilon_{\text{radial}}^{\text{acc}}$ and axial $\varepsilon_{\text{axial}}^{\text{acc}}$ strain with the number of cycles N of samples subjected to cyclic vertical load; the average mean stress is $p_0' = 200$ kPa, and the stress amplitude is $\Delta q = 60$ kPa; (b) zero-lateral strain test: evolution of mean stress p', void ratio e, and coefficient of earth pressure at rest K_0 in an oedometer cell with average vertical stress $\sigma_v = 100$ kPa and subjected to a cyclic vertical stress $\Delta\sigma_v = 20$ kPa; boxes in e-p' space correspond to cycles $N = 2^5, 2^8, 2^{11}, 2^{15}, 2^{18}$, and 2^{19}

Example 1: Flexible Foundation Subjected to Repetitive Loading

Consider a flexible shallow foundation on sand subjected to a static vertical load followed by repetitive vertical loading (Fig. 5). The subsurface is modeled using 2,870 four-node plane strain elements with full integration. The numerically predicted footing bearing capacity is $Q_{\text{ult}} = 750$ kPa and agrees well with Terzaghi's bearing capacity.

The stress and strain fields due to the static load $Q_A = Q_{\text{ult}}/3 = 250$ kPa and the first load cycle $\Delta Q = 0.05 \cdot Q_A = 12.5$ kPa are calculated using the modified Cam clay model parameters in Table 1. Fig. 5(a) shows the evolution of the footing vertical displacement with the number of cycles. The repetitive load causes an additional vertical displacement of 6 mm after $N = 100{,}000$ cycles, and there is an associated decrease in void ratio underneath the footing [Fig. 5(b)].

The average void ratio from the surface to an influence depth similar to the footing width $z = B_f = 1$ m is $e_A = 0.689$. Assuming that repetitive loading compacts the soil to its terminal void ratio $e_\infty = 0.577$, the maximum volumetric change the soil can experience in this zone is $\Delta\varepsilon_v^{\max} = (e_A - e_\infty)/(1 + e_A) = 0.066$. This volumetric change is equivalent to a maximum settlement $\delta_{\max} = B_f \cdot \Delta\varepsilon_v^{\max} = 66$ mm, which is 11 times larger than the additional vertical displacement calculated after $N = 100{,}000$ cycles. This comparison between an upper-bound estimate and numerical results suggest that footing settlement may still accumulate after the maximum number of cycles analyzed.

The zone of high stress obliquity $\eta = q/p$ grows from the footing center toward the edge underneath the footing [Fig. 5(c)]; therefore, while the static vertical load remains constant, the cyclic load gradually brings the subsurface soil to critical stress obliquity $\eta = M$. However, sediment densification increases the preconsolidation pressure pc and consequently enlarges the yield surface; therefore, cyclic loading does not necessarily bring the system closer to failure in this case.

The factor of safety $FS = Q_{\text{ult}}/Q_A$ and the cyclic load amplitude ΔQ affect the footing response to the repetitive load (Fig. 6). The settlement of the footing center point increases with the applied static load Q_A and with the cyclic load amplitude ΔQ (i.e., lower factor of safety).

The application of an additional static horizontal load on the footing $T_A \sim Q_A/6$ does not increase surface settlements. However, horizontal displacements increase proportional to the cyclic load amplitude ΔQ during repetitive loading [Fig. 6(b)].

Example 2: Rigid Footing Subjected to Repetitive Eccentric Load

Gravity-based foundations are preferred for wind turbines onshore and offshore in shallow water (Byrne and Houlsby 2006). The repetitive wind load adds an overturning moment to the foundation. Consider a $B_f = 14$-m-wide footing buried $D_f = 2.5$ m deep, and made of concrete density $\gamma_f = 25\,\text{kN/m}^3$ and Young's modulus $E_f = 30$ GPa. A static vertical force $P_A = 10$ MN/m is applied at the center of the footing. The cyclic overturning moment is modeled as an eccentric cyclic force $\Delta P = 0.5$ MN/m applied 3.5 m away from the centerline.

The sand subsurface is modeled with 4,400 four-node plane strain elements with full integration. The stress and strain fields induced by the static load and the first load cycle are calculated using the modified Cam clay model (sand model parameters in Table 1). For these parameters, the maximum numerically predicted normal force the footing can sustain is approximately $P_A^{\text{ult}} = 60$ MN/m.

Fig. 7 shows (a) vertical displacements induced by the static force and the first load cyclic, and the additional displacement due to the

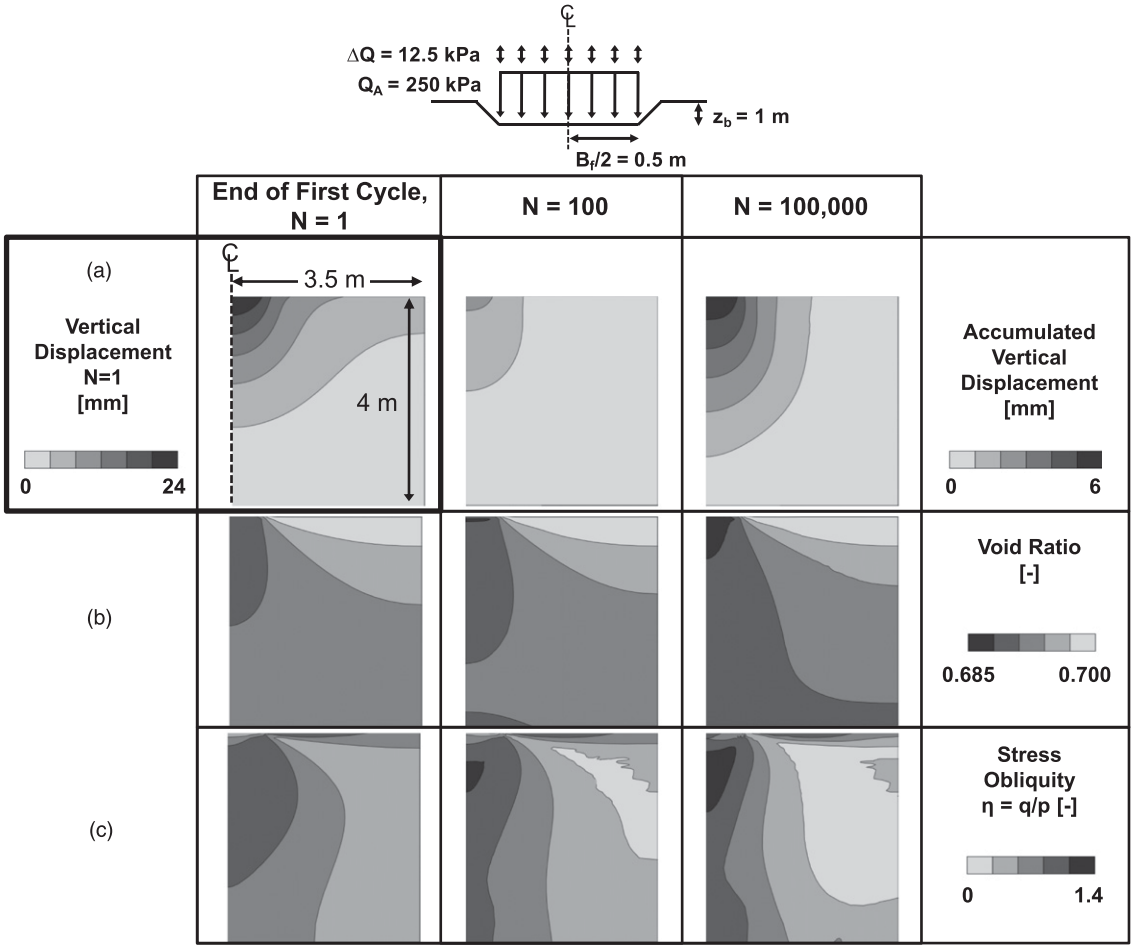

Fig. 5. Flexible shallow foundation subjected to vertical repetitive loading: (a) accumulation of vertical displacement; distribution of (b) void ratio and (c) stress obliquity η for load cycles $N = 1, 100, 100{,}000$. The static and the cyclic loads are $Q_A = Q_{ult}/3 = 250$ kPa and $\Delta Q = 0.1 \cdot Q_A = 12.5$ kPa for a bearing capacity $Q_{ult} \sim 750$ kPa

cyclic force after $N = 100{,}000$ cycles; (b) the void ratio and (c) the stress obliquity for load cycles $N = 1$ and $N = 100{,}000$. It can be seen that the cyclic force induces densification, footing settlement, and rotation.

The horizontal and vertical displacement of the footing center point B as well as the footing rotation, the difference between the vertical displacements of points A and C divided by the footing width B_f, are shown in Fig. 8 for various static factors of safety $FS = P_{ult}/P_A$ and cyclic force amplitude $\Delta P/P_A$. Displacements and rotations increase as the factor of safety P_{ult}/P_A decreases and the cyclic force amplitude $\Delta P/P_A$ increases. The continuous accumulation of both horizontal displacement and rotation suggests that the footing may experience long-term ratcheting behavior.

The volumetric accumulation is slow, and the lowest void ratio reached after $N = 100{,}000$ cycles is $e = 0.68 > e_\infty = 0.577$ (Fig. 7). Hence, the footing may continue settling and rotating with increasing load cycles until the soil approaches its terminal void ratio everywhere beneath the footing depth of influence where the strain from the first load cycle exceeds the elastic threshold strain.

Discussion

The proposed numerical scheme and other recently developed models with empirical strain accumulation are summarized and compared in Table 2. The simple and robust numerical scheme proposed in this study presents some clear advantages with respect to other methods. The constitutive model and accumulation functions capture proper initial and asymptotic trends, such as the nonlinear response to the initial load and the first load cycle, terminal density, and ratcheting behavior for high stress obliquity. The static load and the first load cycle must be simulated with constitutive models that yield plastic strain.

The accumulated strain is explicitly defined, and the solution converges fast, particularly when the cyclic component of the boundary load is low compared with the static component. The formulation can be modified to account for repetitive displacement boundary conditions. The algorithm applies to relatively constant repetitive load characteristics and stress conditions, yet the state of stress and the strain amplitudes change during the application of repetitive loads (a validation of Miner's rule for sands is presented in Wichtmann et al. 2010a). Problems that involve sequences of drained and undrained loads cannot be accurately tested owing to the lack of experimental data. However, experimental results from drained cyclic multidirectional simple shear tests (Wichtmann et al. 2007) and drained cyclic true triaxial tests (Yamada and Ishihara 1982) suggest that changes through the loading history can alter the strain accumulation rate.

In weakly constrained problems, such as foundation problems, the stress field is quite independent of the constitutive model;

J. Geotech. Geoenviron. Eng. 2014.140.

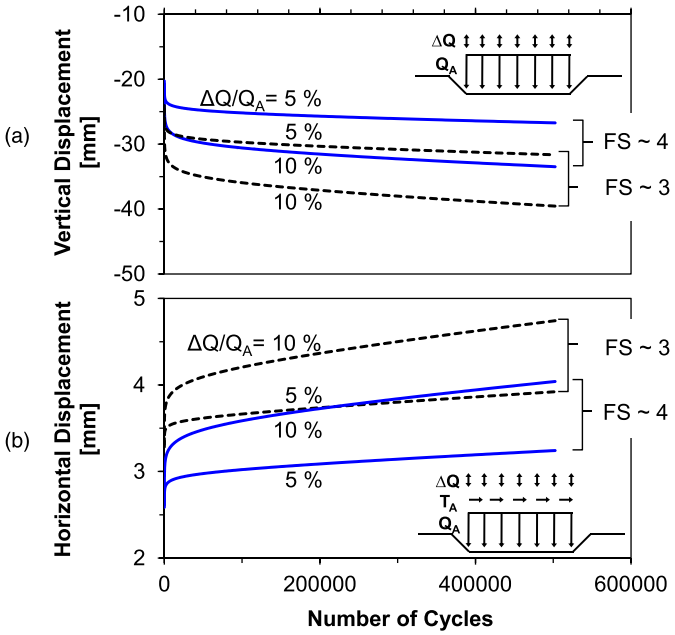

Fig. 6. Displacement evolution of a flexible shallow foundation subjected to repetitive loading: (a) vertical displacement measured at the center of the footing for static vertical loads $Q_A = 250\,\text{kPa}\,(FS = Q_A^{\text{ult}}/Q_A \sim 3)$ and $Q_A = 190\,\text{kPa}\,(FS \sim 4)$, and cyclic vertical loads ΔQ; (b) horizontal displacement caused by an additional static horizontal load $T_A = 40\,\text{kPa}\,(FS \sim 3)$ and $T_A = 30\,\text{kPa}\,(FS \sim 4)$; note: the static horizontal load T_A does not change the vertical displacement

however, this is not the case for strains. Proper calibration of the constitutive model (static settlement and first cycle) plays an important role in the anticipated long-term response under repetitive loading.

The hybrid constitutive model with empirical strain accumulation described here adds five parameters (a, b, c, e_∞, and ε_{el}) to the parameters needed for the constitutive model used to analyze the static and first-cycle loads. Additional calibration flexibility can be gained by relaxing these parameters; for example, accommodating a, b, and c as a function of the stress obliquity η or defining the terminal void ratio as a function rather than as a constant value.

New test protocols are needed (1) to accurately predict the first cycle strains $\varepsilon_v|_{N=1}$ and $\varepsilon_q|_{N=1}$ and (2) to properly calibrate the accumulation functions with emphasis on the determination of asymptotic conditions. In particular, strain accumulation functions should be carefully calibrated to match the measured incremental and cumulative strain trends. The calibrated model can be tested against the evolution of vertical and horizontal strains in a triaxial condition, and the evolution of the coefficient of earth pressure at rest K_0 under zero-lateral strain boundary conditions. Model calibration also requires experimental data to determine elastic threshold strains and terminal densities.

The proposed methodology can be extended to other repetitive actions that can cause cumulative soil deformation, including temperature oscillations (Campanella and Mitchell 1968; Towhata et al. 1993), freeze-thaw cycles (Qi et al. 2006), wet-dry cycles (Albrecht and Benson 2001; Tripathy and Subba Rao 2009), and cyclic pore fluid changes (Musso et al. 2003).

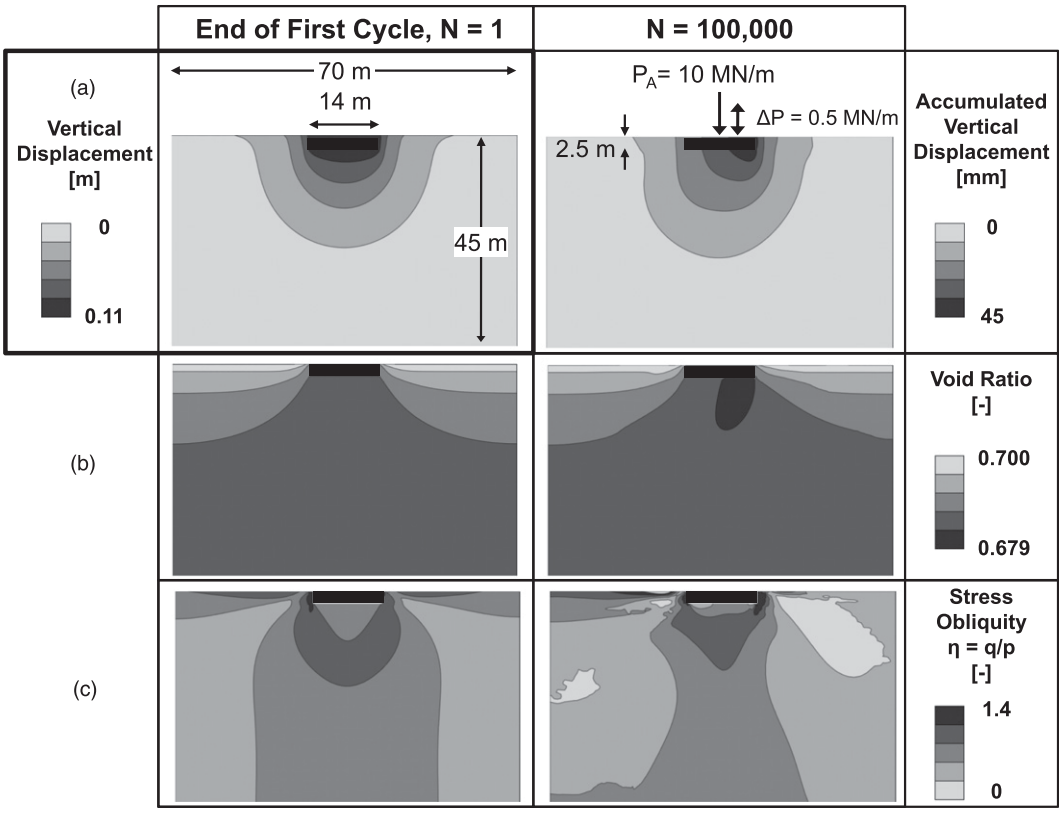

Fig. 7. Rigid foundation subjected to repetitive eccentric load: (a) vertical displacement; distribution of (b) void ratio and (c) stress obliquity η for load cycles $N = 1$ and $N = 100{,}000$; the cyclic force ΔP is applied at $e_x = 3.5$ m from the footing center; note: the maximum force the footing can sustain is estimated as $P_A^{\text{ult}} = 60\,\text{MN/m}$

J. Geotech. Geoenviron. Eng. 2014.140.

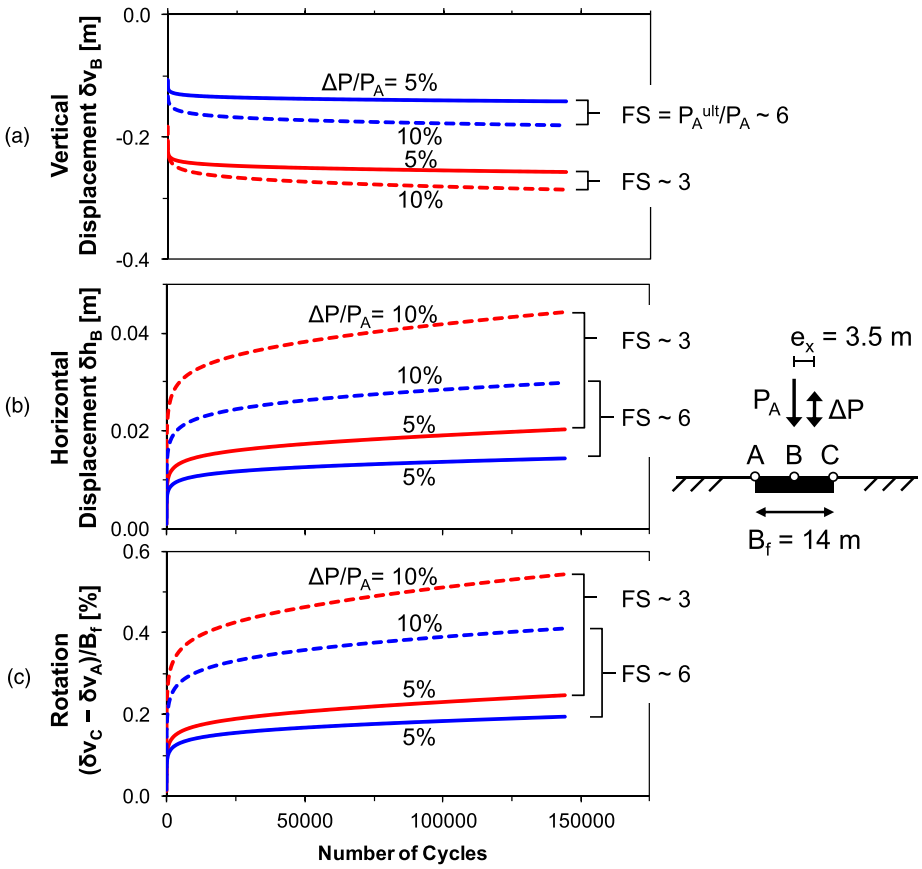

Fig. 8. Rigid foundation subjected to repetitive eccentric load at $e_x = 3.5\,\text{m}$: (a) vertical displacement; (b) horizontal displacement; and (c) rotation $(\delta v_C - \delta v_A)/B_f$ for static loads $P_A = 20\,\text{kN/m}$ $(FS = P_A^{\text{ult}}/P_A \sim 3)$ and $P_A = 10\,\text{kN/m}$ $(FS \sim 6)$, and cyclic loads ΔP; note: the maximum force the footing can sustain is estimated as $P_A^{\text{ult}} = 60\,\text{MN/m}$

Table 2. Comparison of Accumulation Models

Model Feature	Suiker and de Borst (2003)	Niemunis et al. (2005)	Francois et al. (2010)	This study
Definition of accumulated strain	Frictional sliding and volumetric compaction	Intensity times direction	Frictional sliding and volumetric compaction	Volumetric and shear strain
Consideration of the cyclic load amplitude	Pseudostatic application of the maximum expected boundary load	Strain amplitude from first cycle	Wave propagation model	Strain amplitude from first cycle
Account for threshold strains	No	No	No	Yes
Model for the initial state	Elastoplastic model analogous to cyclic model	Hypoplastic with intergranular strain	N/A (one-step calculation)	Modified Cam clay (it can accommodate any model)
Failure criterion	Drucker-Prager	Matsuoka-Nakai	N/A	Modified Cam clay
Predefined cyclic flow rule	No	Modified Cam clay direction	No	No
Accounts for terminal density	Yes	No	No	Yes
Stress-dependent elastic stiffness	Yes	Yes	Yes	Yes
Accumulation functions				
Stress dependent	Yes	Yes	Yes	Yes
Number of cycles	Yes	Yes	Yes	Yes
Depend on the previous-step accumulated strain	Yes	No (depend on first cycle)	Yes	No (depend on first cycle)
Initial void ratio effect	No	Yes	No	Not explicitly

Conclusions

A numerical scheme is proposed to analyze the long-term behavior of boundary value problems with a large number of mechanical load cycles. The hybrid approach involves a mechanical constitutive model to analyze the static load and the first load cycle and empirical strain accumulation functions to track the deformation accumulation during repetitive loading. The empirical functions predict volumetric and shear strain accumulation as a function of the plastic strain during the first load cycle, the obliquity and amplitude of the cyclic load, and the number of load cycles.

The numerical scheme satisfies initial conditions and asymptotic trends. In particular, the cyclic flow rule, obtained from dividing the volumetric strain by the shear strain, (1) satisfies the modified Cam clay model's flow rule for the first cycle and (2) approaches zero for a high number of cycles to account for terminal density while allowing for continuous shear strain accumulation, or ratcheting.

Accumulation functions add five new variables that require new test protocols for calibration. The physical admissibility of constitutive parameters can be pretested by modeling triaxial and zero-lateral strain tests.

Numerical simulations of a shallow foundation subjected to vertical and horizontal static loads and repetitive vertical load show the accumulation of vertical and horizontal displacements and stress redistribution with the number of load cycles. On the other hand, the analysis of a rigid foundation subjected to repetitive eccentric load shows that the footing experiences cumulative settlement and rotation; trends are more pronounced as the factor of safety decreases and the cyclic load amplitude increases.

Acknowledgments

Support for this research was provided by the Fulbright U.S.-Chile Equal Opportunities Scholarship Program, the U.S. Department of Energy, and the Goizueta Foundation. Francisco Santamarina edited the manuscript.

References

ABAQUS 6.10 [Computer software]. Providence, RI, Dassault Systèmes Simulia.

Albrecht, B. A., and Benson, C. H. (2001). "Effect of desiccation on compacted natural clays." *J. Geotech. Geoenviron. Eng.*, 10.1061/(ASCE)1090-0241(2001)127:1(67), 67–75.

Alonso-Marroquin, F., and Herrmann, H. J. (2004). "Ratcheting of granular materials." *Phys. Rev. Lett.*, 92(5), 054301.

Barksdale, R. D. (1972). "Laboratory evaluation of rutting in basecourse materials." *Proc., 3rd Int. Conf. on Structural Design of Asphalt Pavements*, International Society for Asphalt Pavements, Lino Lakes, MN, 161–174.

Bouckovalas, G., Whitman, R. V., and Marr, W. A. (1984). "Permanent displacement of sand with cyclic loading." *J. Geotech. Engrg.*, 10.1061/(ASCE)0733-9410(1984)110:11(1606), 1606–1623.

Brown, S. F. (1974). "Repeated load testing of a granular material." *J. Geotech. Engrg. Div.*, 100(7), 825–841.

Byrne, B. W., and Houlsby, G. T. (2006). "Assessing novel foundation options for offshore wind turbines." *Proc., World Maritime Technology Conf.*, International Council on Combustion Engines, Frankfurt, Germany, ⟨http://www.lonestarbit.com/mining/Offshore_wind_foundation.pdf⟩.

Campanella, R. G., and Mitchell, J. K. (1968). "Influence of temperature variations on soil behavior." *J. Soil Mech. and Found. Div.*, 94(3), 709–734.

Chang, C. S., and Whitman, R. V. (1988). "Drained permanent deformation of sand due to cyclic loading." *J. Geotech. Engrg.*, 10.1061/(ASCE)0733-9410(1988)114:10(1164), 1164–1180.

Dafalias, Y. F., and Herrmann, L. R. (1986). "Bounding surface plasticity. II: Application to isotropic cohesive soils." *J. Eng. Mech.*, 10.1061/(ASCE)0733-9399(1986)112:12(1263), 1263–1291.

Diyaljee, V. A., and Raymond, G. P. (1982). "Repetitive load deformation of cohesionless soil." *J. Geotech. Engrg. Div.*, 108(10), 1215–1229.

Dobry, R., and Swiger, W. F. (1979). "Threshold strain and cyclic behavior of cohesionless soils." *Proc., 3rd ASCE/EMDE Specialty Conf.*, ASCE, Reston, VA, 521-525.

François, S., Karg, C., Haegeman, W., and Degrande, G. (2010). "A numerical model for foundation settlements due to deformation accumulation in granular soils under repeated small amplitude dynamic loading." *Int. J. Numer. Anal. Methods Geomech.*, 34(3), 273–296.

Gajo, A., and Muir Wood, D. (1999). "Severn-Trent sand: A kinematic-hardening constitutive model: The q-p formulation." *Geotechnique*, 49(5), 595–614.

Garcia-Rojo, R., and Herrmann, H. J. (2005). "Shakedown of unbound granular material." *Granul. Matter*, 7(2–3), 109–118.

Gidel, G., Hornych, P., Chauvin, J. J., Breysse, D., and Denis, A. (2001). "A new approach for investigating the permanent deformation behaviour of unbound granular material using the repeated load triaxial apparatus." *Bulletin of the Laboratory of Bridges and Roads*, 233(4), 5–21.

Kaggwa, W. S., Booker, J. R., and Carter, J. P. (1991). "Residual strains in calcareous sand due to irregular cyclic loading." *J. Geotech. Engrg.*, 10.1061/(ASCE)0733-9410(1991)117:2(201), 201–218.

Lackenby, J. (2006). "Triaxial behaviour of the ballast and the role of confining pressure under cyclic loading." Ph.D. thesis, Univ. of Wollongong, Wollongong, NSW, Australia.

Lekarp, F., and Dawson, A. (1998). "Modelling permanent deformation behaviour of unbound granular materials." *Construct. Build. Mater.*, 12(1), 9–18.

Lentz, R. W., and Baladi, G. Y. (1980). "Simplified procedure to characterize permanent strain in sand subjected to cyclic loading." *Proc., Int. Symp. on Soils under Cyclic and Transient Loading*, Balkema, Rotterdam, Netherlands, 89–95.

Lentz, R. W., and Baladi, G. Y. (1981). "Constitutive equation for permanent strain of sand subjected to cyclic loading." *Transp. Res. Rec.*, 810, 50–54.

Marr, W. A., and Christian, J. T. (1981). "Permanent displacements due to cyclic wave loading." *J. Geotech. Engrg. Div.*, 107(8), 1129–1149.

Mróz, Z. (1967). "On the description of anisotropic workhardening." *J. Mech. Phys. Solids*, 15(3), 163–175.

Muir Wood, D. (1990). *Soil behaviour and critical state soil mechanics*, Cambridge University Press, Cambridge, U.K.

Musso, G., Romero Morales, E., Gens, A., and Castellanos, E. (2003). "The role of structure in the chemically induced deformations of FEBEX bentonite." *Appl. Clay Sci.*, 23(1–4), 229–237.

Narsilio, G. A., and Santamarina, J. C. (2008). "Terminal densities." *Geotechnique*, 58(8), 669–674.

Niemunis, A., Wichtmann, T., and Triantafyllidis, T. (2004). "Explicit accumulation model for cyclic loading." *Proc., Int. Conf. on Cyclic Behaviour of Soils and Liquefaction Phenomena*, Taylor & Francis, London, 65–76.

Niemunis, A., Wichtmann, T., and Triantafyllidis, T. (2005). "A high-cycle accumulation model for sand." *Comput. Geotech.*, 32(4), 245–263.

Qi, J., Vermeer, P. A., and Cheng, G. (2006). "A review of the influence of freeze-thaw cycles on soil geotechnical properties." *Permafrost Periglacial Processes*, 17(3), 245–252.

Rondón, H. A., Wichtmann, T., Triantafyllidis, T., and Lizcano, A. (2009). "Comparison of cyclic triaxial behavior of unbound granular material under constant and variable confining pressure." *J. Transp. Eng.*, 10.1061/(ASCE)TE.1943-5436.0000009, 467–478.

Santamarina, J. C., Klein, K. A., and Fam, M. A. (2001). *Soils and Waves*, Wiley, New York.

Sawicki, A., and Swidzinski, W. (1989). "Mechanics of a sandy subsoil subjected to cyclic loadings." *Int. J. Numer. Anal. Methods Geomech.*, 13(5), 511–529.

Sawicki, A., and Swidzinski, W. (1995). "Cyclic compaction of soils, grains and powders." *Powder Technol.*, 85(2), 97–104.

Suiker, A. S. J., and de Borst, R. (2003). "A numerical model for the cyclic deterioration of railway tracks." *Int. J. Numer. Methods Eng.*, 57(4), 441–470.
Suiker, A. S. J., Selig, E. T., and Frenkel, R. (2005). "Static and cyclic triaxial testing of ballast and subballast." *J. Geotech. Geoenviron. Eng.*, 10.1061/(ASCE)1090-0241(2005)131:6(771), 771–782.
Sweere, G. T. H. (1990). "Unbound granular bases for roads." Ph.D. thesis, Delft Univ. of Technology, Delft, Netherlands.
Towhata, I., Kuntiwattanaku, P., Seko, I., and Ohishi, K. (1993). "Volume change of clays induced by heating as observed in consolidation tests." *Soils Found.*, 33(4), 170–183.
Tripathy, S., and Subba Rao, K. S. (2009). "Cyclic swell-shrink behaviour of a compacted expansive soil." *Geotech. Geol. Eng.*, 27(1), 89–103.
Tseng, K.-H., and Lytton, R. L. (1989). "Prediction of permanent deformation in flexible pavement materials." *Implication of Aggregates in the Design, Construction, and Performance of Flexible Pavements, STP 1016*, ASTM, West Conshohocken, PA, 154–154.
Vucetic, M., and Dobry, R. (1991). "Effect of soil plasticity on cyclic response." *J. Geotech. Engrg.*, 10.1061/(ASCE)0733-9410(1991)117:1(89), 89–107.
Wichtmann, T. (2005). "Explicit accumulation model for non-cohesive soils under cyclic loading." Ph.D. thesis, Ruhr Univ. Bochum, Bochum, Germany.
Wichtmann, T., Niemunis, A., and Triantafyllidis, T. (2006). "Experimental evidence of a unique flow rule of non-cohesive soils under high-cyclic loading." *Acta Geotech.*, 1(1), 59–73.
Wichtmann, T., Niemunis, A., and Triantafyllidis, T. (2007). "On the influence of the polarization and the shape of the strain loop on strain accumulation in sand under high-cyclic loading." *Soil. Dyn. Earthquake Eng.*, 27(1), 14–28.
Wichtmann, T., Niemunis, A., and Triantafyllidis, T. (2010a). "Strain accumulation in sand due to drained cyclic loading: On the effect of monotonic and cyclic preloading (Miner's rule)." *Soil. Dyn. Earthquake Eng.*, 30(8), 736–745.
Wichtmann, T., Rondon, H. A., Niemunis, A., Triantafyllidis, T., and Lizcano, A. (2010b). "Prediction of permanent deformations in pavements using a high-cycle accumulation model." *J. Geotech. Geoenviron. Eng.*, 10.1061/(ASCE)GT.1943-5606.0000275, 728–740.
Yamada, Y., and Ishihara, K. (1982). "Yielding of loose sand in three-dimensional stress conditions." *Soils Found.*, 22(3), 15–31.
Youd, T. L. (1972). "Compaction of sands by repeated shear straining." *J. Soil Mech. and Found. Div.*, 98(7), 709–725.
Zhang, H. W., Heeres, O. M., Borst, R. d., and Schrefler, B. A. (2001). "Implicit integration of a generalized plasticity constitutive model for partially saturated soil." *Eng. Computat.*, 18(1/2), 314–336.